

Mechanism of Hydride Donor Generation Using a Ru(II) Complex Containing an NAD⁺ Model Ligand: Pulse and Steady-State Radiolysis Studies

Dmitry E. Polyansky,[†] Diane Cabelli,[†] James T. Muckerman,[†] Takashi Fukushima,[‡] Koji Tanaka,[‡] and Etsuko Fujita^{*†}

Chemistry Department, Brookhaven National Laboratory, Upton, New York 11973-5000, and Institute for Molecular Science, 5-1 Higashiyama, Myodaiji, Okazaki, Aichi 444-8787, Japan

Received October 30, 2007

The mechanistic pathways of formation of the NADH-like [Ru(bpy)₂(pbnHH)]²⁺ species from [Ru(bpy)₂(pbn)]²⁺ were studied in an aqueous medium. Formation of the one-electron-reduced species as a result of reduction by a solvated electron ($k = 3.0 \times 10^{10} \text{ M}^{-1} \text{ s}^{-1}$) or CO₂^{•-} ($k = 4.6 \times 10^9 \text{ M}^{-1} \text{ s}^{-1}$) or reductive quenching of an MLCT excited state by 1,4-diazabicyclo[2.2.2]octane ($k = 1.1 \times 10^9 \text{ M}^{-1} \text{ s}^{-1}$) is followed by protonation of the reduced species ($\text{p}K_{\text{a}} = 11$). Dimerization ($k_{\text{r}_a} = 2.2 \times 10^8 \text{ M}^{-1} \text{ s}^{-1}$) of the singly reduced protonated species, [Ru(bpy)₂(pbnH[•])]²⁺, followed by disproportionation of the dimer as well as the cross reaction between the singly reduced protonated and nonprotonated species ($k_{\text{b}} = 1.2 \times 10^8 \text{ M}^{-1} \text{ s}^{-1}$) results in the formation of the final [Ru(bpy)₂(pbnHH)]²⁺ product together with an equal amount of the starting complex, [Ru(bpy)₂(pbn)]²⁺. At 0.2 °C, a dimeric intermediate, most likely a π -stacking dimer, was observed that decomposes thermally to form an equimolar mixture of [Ru(bpy)₂(pbnHH)]²⁺ and [Ru(bpy)₂(pbn)]²⁺ (pH < 9). The absence of a significant kinetic isotope effect in the disproportionation reaction of [Ru(bpy)₂(pbnH[•])]²⁺ and its conjugate base (pH > 9) indicates that disproportionation occurs by a stepwise pathway of electron transfer followed by proton transfer.

Introduction

It has been widely accepted that global climate change is associated with growing carbon dioxide emissions. Among several chemical approaches considered to mitigate CO₂, one of the most desirable methods is chemical conversion of carbon dioxide to compounds such as CO, formic acid, or methanol that can be utilized as precursors in synthetic reactions or as fuels.¹ However, the desired reactions are thermodynamically highly uphill and require substantial input of energy and special catalysts. One of the approaches to develop such systems is to mimic natural photosystems (e.g., Photosystem I), where carbon dioxide is fixed in the Calvin cycle to produce sugars by an NADH coenzyme and a high energy ATP molecule as a result of light absorption.² The electrons necessary to produce reducing equivalents are

drawn from the oxidation of water by Photosystem II, and the driving force for the reaction is provided through the absorption of visible light. One of the key components of Photosystem I is the NADH cofactor that serves as a shuttle for reducing equivalents and acts as a source of two electrons and a proton. Because of this attractive property, photochemical and thermal reactions mediated by NADH model compounds such as 1-benzyl-1,4-dihydronicotinamide (BNAH) or 10-methylacridan, for example, the reduction of alkyl halides, olefins, ketones, and photoinduced electron transfer, have been extensively studied.^{3,4} However, most of the reactions mediated with NADH models are limited to stoichiometric reactions, partially due to the facile dimerization of the radical species NAD[•] formed either by the reduction of NAD⁺ or by oxidation of NADH, followed by deprotonation. The dimerization can be avoided by (1) removing the C-centered radical species through a rapid reduction³ or oxidation, or (2) attaching a bulky group near the C-centered radical.

* E-mail: fujita@bnl.gov.

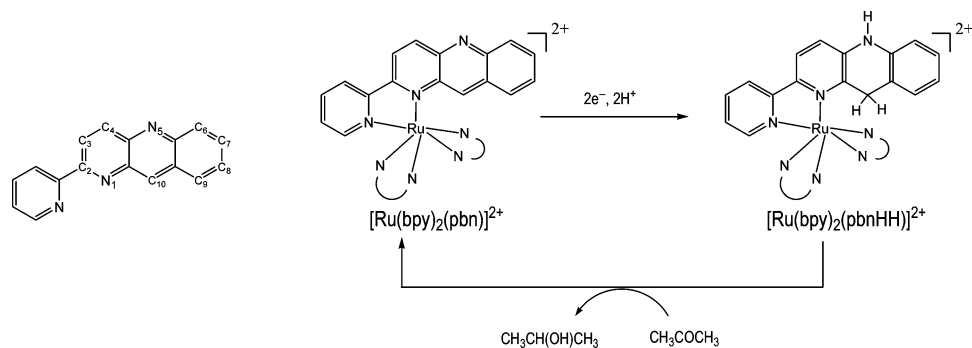
[†] Brookhaven National Laboratory.

[‡] Institute for Molecular Science.

(1) In Basic Research Needs for Solar Energy Utilization, Report on the Basic Energy Sciences Workshop On Solar Energy Utilization, April 18–21, 2005.

(2) Bassham, J. A. *Photosynth. Res.* **2003**, *76*, 35–52.

(3) Ishikawa, M.; Fukuzumi, S. *J. Am. Chem. Soc.* **1990**, *112*, 8864–8870.

Scheme 1. Ligand (pbn) Atom Numbering Scheme and Electrochemical Reduction of $[\text{Ru}(\text{bpy})_2(\text{pbn})](\text{PF}_6)_2$ in Aqueous Acetone Solution

Divalent and trivalent metal ions such as Mg^{2+} and Sc^{3+} have been proven to accelerate the electron or hydride transfer rate from NADH analogues to oxidants.^{5–7} Transition metal complexes with a BNAH ligand such as $[\text{Ru}(\text{tpy})(\text{bpy})(\text{BNAH})]^{2+}$ or $[\text{Re}(\text{bpy})(\text{CO})_3(\text{BNAH})]^+$ (tpy = 2,2',6',2''terpyridine, bpy = 2,2'-bipyridine) have been prepared.⁸ The C-centered hydride donor abilities of these complexes were enhanced through the deprotonation of the carbamoyl group of the BNAH ligand in the presence of a base.⁸ Therefore, the properties of NAD^+/NADH analogues can be tuned by electronic structural changes through the interaction of the analogues with metal ions/complexes. Together with the fact that transition metal complexes absorb light efficiently over a wide spectral range, have long-lived excited states, and have multiple oxidation states, artificial NADH analogues containing transition metals are attractive for use as photocatalysts for fuels production and reduction of organic molecules.

Previously, some of us have reported the electrocatalytic ability of $[\text{Ru}(\text{bpy})_2(\text{pbn})]^{2+}$ (pbn = 2-(2-pyridyl)benzo[*b*]-

1,5-naphthyridine) for the reduction of acetone to isopropanol, presumably with $[\text{Ru}(\text{bpy})_2(\text{pbnHH})]^{2+}$ (pbnHH = 5,10-dihydro-2-(2-pyridyl)benzo[*b*]-1,5-naphthyridine) as the key intermediate as shown in Scheme 1.⁹ Recently, we have demonstrated that $[\text{Ru}(\text{bpy})_2(\text{pbnHH})]^{2+}$ is cleanly formed by the reductive quenching of the metal-to-ligand charge-transfer (MLCT) excited-state of $[\text{Ru}(\text{bpy})_2(\text{pbn})]^{2+}$ by triethylamine upon irradiation with visible light ($<600\text{ nm}$)¹⁰ with the quantum yield for the formation of $[\text{Ru}(\text{bpy})_2(\text{pbnHH})]^{2+}$ of 0.21 at $\lambda = 355 \pm 6\text{ nm}$. These results open new opportunities for the photochemical generation of strong hydride donors for the *catalytic* hydrogenation of organic molecules (and hopefully CO_2 and related species) by visible-light irradiation as Nature does. This finding has also prompted us to carry out more detailed studies on the mechanism of the photochemical formation of the $[\text{Ru}(\text{bpy})_2(\text{pbnHH})]^{2+}$ species. Here we present a comprehensive mechanistic study of $[\text{Ru}(\text{bpy})_2(\text{pbn})]^{2+}$ conversion into $[\text{Ru}(\text{bpy})_2(\text{pbnHH})]^{2+}$ using steady-state and transient radiolytic and photochemical techniques. The observation of pH-dependent kinetics of the second-order decays of the one-electron-reduced species $[\text{Ru}(\text{bpy})_2(\text{pbn}^{\cdot-})]^+$ points toward two key disproportionation pathways to $[\text{Ru}(\text{bpy})_2(\text{pbnHH})]^{2+}$ and $[\text{Ru}(\text{bpy})_2(\text{pbn})]^{2+}$: one pathway involves the formation of a π -stacking dimer of $[\text{Ru}(\text{bpy})_2(\text{pbnH}^{\cdot+})]^{2+}$ (that lives longer than 300 ms at 25 °C), and another pathway likely involves a hydrogen-bonded interaction between $[\text{Ru}(\text{bpy})_2(\text{pbn}^{\cdot-})]^+$ and $[\text{Ru}(\text{bpy})_2(\text{pbnH}^{\cdot+})]^{2+}$.

Experimental Section

Materials. The ligand pbn was prepared from 3-aminoquinoline by a seven-step synthesis using previously published methods.¹ ^1H NMR (500 MHz, CDCl_3): δ 9.07 (s, 1H), 8.90 (d, 1H, $J(\text{H}-\text{H}) = 9.0\text{ Hz}$), 8.79 (dd, 1H, $J(\text{H}-\text{H}) = 4.9$ and 1.8 Hz), 8.72 (d, 1H, $J(\text{H}-\text{H}) = 7.9\text{ Hz}$), 8.63 (d, 1H, $J(\text{H}-\text{H}) = 9.0\text{ Hz}$), 8.28 (d, 1H, $J(\text{H}-\text{H}) = 8.5\text{ Hz}$), 8.12 (d, 1H, $J(\text{H}-\text{H}) = 8.5\text{ Hz}$), 7.92 (td, 1H, $J(\text{H}-\text{H}) = 7.6$ and 1.8 Hz), 7.85 (t, 1H, $J(\text{H}-\text{H}) = 7.6\text{ Hz}$), 7.61 (t, 1H, $J(\text{H}-\text{H}) = 7.3\text{ Hz}$), 7.42 (dd, 1H, $J(\text{H}-\text{H}) = 7.3$ and 4.3 Hz). $[\text{Ru}(\text{bpy})_2(\text{pbn})](\text{PF}_6)_2$ was prepared as previously described⁹ and characterized by NMR, UV-vis, IR, and ES-MS spectroscopy. $[\text{Ru}(\text{bpy})_2(\text{pbnHH})](\text{PF}_6)_2$ was prepared in the following way.

- (4) (a) For example: Fukuzumi, S. In *Advances in Electron-Transfer Chemistry*; Mariano, P. S., Ed.; JAI Press Inc.: Greenwich, CT, 1992; pp 67–175. (b) Gêbicki, J.; Marcinek, A.; Zielonka, J. *Acc. Chem. Res.* **2004**, *37*, 379–386. (c) Fukuzumi, S.; Inada, O.; Suenobu, T. *J. Am. Chem. Soc.* **2003**, *125*, 4808–4816. (d) Zhu, X.-Q.; Yang, Y.; Zhang, M.; Cheng, J.-P. *J. Am. Chem. Soc.* **2003**, *125*, 15298–15299. (e) Nakanishi, I.; Ohkubo, K.; Fujita, S.; Fukuzumi, S.; Konishi, T.; Fujitsuka, M.; Ito, O.; Miyata, N. *J. Chem. Soc., Perkin Trans. 2* **2002**, 1829. (f) Fukuzumi, S.; Imahori, H.; Okamoto, K.; Yamada, H.; Fujitsuka, M.; Ito, O.; Guldi, D. M. *J. Phys. Chem. A* **2002**, *106*, 1903. (g) Reichebach-Klinke, R.; Kruppa, M.; König, B. *J. Am. Chem. Soc.* **2002**, *124*, 12999. (h) Zhu, X.-Q.; Li, H.-R.; Li, Q.; Ai, T.; Lu, J.-Y.; Yang, Y.; Cheng, J.-P. *Chem.—Eur. J.* **2003**, *9*, 871. (i) Lu, Y.; Zhao, Y.; Handoo, K. L.; Parker, V. D. *Org. Biomol. Chem.* **2003**, *1*, 173. (j) Gran, U. *Tetrahedron* **2003**, *59*, 4303. (k) Zhu, X.-Q.; Cao, L.; Liu, Y.; Yang, Y.; Lu, J.-Y.; Wang, J.-S.; Cheng, J.-P. *Chem.—Eur. J.* **2003**, *9*, 3937. (l) Mikata, Y.; Aida, S.; Yano, S. *Org. Lett.* **2004**, *6*, 2921. (m) Selvaraju, C.; Ramamurthy, P. *Chem.—Eur. J.* **2004**, *10*, 2253. (n) Ritter, S. C.; Eiblmaier, M.; Michlova, V.; König, B. *Tetrahedron* **2005**, *61*, 5241. (o) Buck, H. *Int. J. Quantum Chem.* **2005**, *101*, 389. (p) Ishitani, O.; Inoue, N.; Kojie, K.; Ibusuki, T. *J. Chem. Soc., Chem. Commun.* **1994**, 367–368. (q) Kobayashi, A.; Sakamoto, K.; Ishitani, O. *Inorg. Chem. Commun.* **2005**, *8*, 365–367. (r) Tanaka, M.; Ohkubo, K.; Fukuzumi, S. *J. Am. Chem. Soc.* **2006**, *128*, 12372–12373. (s) Yuasa, J.; Yamada, S.; Fukuzumi, S. *J. Am. Chem. Soc.* **2006**, *128*, 14938–14948. (5) Fukuzumi, S.; Yuasa, J.; Satoh, N.; Suenobu, T. *J. Am. Chem. Soc.* **2004**, *126*, 7585–7594. (6) Yuasa, J.; Suenobu, T.; Ohkubo, K.; Fukuzumi, S. *Chem. Commun.* **2003**, 1070–1071. (7) Fukuzumi, S.; Yuasa, J.; Suenobu, T. *J. Am. Chem. Soc.* **2002**, *124*, 12566–12573. (8) Kobayashi, A.; Konno, H.; Sakamoto, K.; Sekine, A.; Ohashi, Y.; Iida, M.; Ishitani, O. *Chem.—Eur. J.* **2005**, *11*, 4219–4226.

(9) Koizumi, T.; Tanaka, K. *Angew. Chem., Int. Ed.* **2005**, *44*, 5891–5894.

(10) Polyansky, D.; Cabelli, D.; Muckerman, J. T.; Fujita, E.; Koizumi, T.; Fukushima, T.; Wada, T.; Tanaka, K. *Angew. Chem., Int. Ed.* **2007**, *46*, 4169–4172.

Addition of an aqueous solution of $\text{Na}_2\text{S}_2\text{O}_4$ (19 mg, $10.7 \mu\text{mol}$ in 5 mL) to a degassed acetonitrile solution of $[\text{Ru}(\text{bpy})_2(\text{pbn})](\text{PF}_6)_2$ (49 mg, $5.1 \mu\text{mol}$ in 20 mL) caused a rapid change of the solution color from red-brown to orange. After the mixture was stirred for 2 h at room temperature, the solution was concentrated to ca. 1 mL by a rotary evaporator. Addition of an aqueous solution of NH_4PF_6 to the solution precipitated orange microcrystals, which were collected and dried in vacuo (38 mg, 78% yield). HR-ESI-MS: $m/z = 336.5764$ $[\text{M} - 2\text{PF}_6]^{2+}$. Elemental analysis: $\text{C}_{37}\text{H}_{29}\text{F}_{12}\text{N}_7\text{O}_2\text{Ru}\cdot\text{H}_2\text{O}$: C, 45.41; H, 2.99; N, 10.02. Found; C, 45.48; H, 3.18; N, 9.70. UV-vis in CH_3CN , λ_{max} , nm (ϵ , $\text{mM}^{-1}\text{cm}^{-1}$): 236 (43.4), 254 (34.0), 288 (88.8), 350 (19.3), 372 (18.1), 390 (15.9), 440 (8.7), 526 (7.2). ^1H NMR (500 MHz, acetone- d_6): δ 8.83 (t, 2H, $J(\text{H-H}) = 7.8$ Hz), 8.82 (d, 2H, $J(\text{H-H}) = 7.8$ Hz), 8.68 (s, 1H, pbnHH-NH), 8.64 (d, 1H, $J(\text{H-H}) = 5.4$ Hz), 8.52 (d, 1H, $J(\text{H-H}) = 8.3$ Hz), 8.44 (d, 1H, $J(\text{H-H}) = 8.8$ Hz, pbnHH- H^3), 8.17–8.24 (m, 5H), 8.07 (t, 1H, $J(\text{H-H}) = 7.8$ Hz), 7.98 (d, 1H, $J(\text{H-H}) = 5.4$ Hz), 7.84 (d, 1H, $J(\text{H-H}) = 4.9$ Hz), 7.68 (d, 1H, $J(\text{H-H}) = 5.4$ Hz), 7.60–7.66 (m, 3H), 7.52 (t, 1H, $J(\text{H-H}) = 6.8$ Hz), 7.41 (d, 1H, $J(\text{H-H}) = 8.8$ Hz, pbnHH- H^4), 7.33 (t, 1H, $J(\text{H-H}) = 6.3$ Hz), 7.00 (t, 1H, $J(\text{H-H}) = 7.3$ Hz, pbnHH- H^8), 6.71 (d, 1H, $J(\text{H-H}) = 7.8$ Hz, pbnHH- H^9), 6.67 (t, 1H, $J(\text{H-H}) = 7.8$ Hz, pbnHH- H^7), 6.18 (d, 1H, $J(\text{H-H}) = 7.3$ Hz, pbnHH- H^6), 4.19 (d, 1H, $J(\text{H-H}) = 21$ Hz, pbnHH- H^{10}), 3.18 (d, 1H, $J(\text{H-H}) = 21$ Hz, pbnHH- H^{10}).

All chemicals used were of reagent grade and used without further purification except acetonitrile (CH_3CN) and triethylamine (Et_3N). CH_3CN and Et_3N were purified in the published manner,¹¹ stored under vacuum over an activated molecular sieve and NaK, respectively, and vacuum-distilled before use. Aqueous solutions were prepared with distilled water that had been passed through a Millipore ultrapurification system. Blanket gases (N_2O , Ar) were UHP grade (99.999%). Solutions for kinetic isotope studies were prepared from D_2O (99.96% D), D_3PO_4 (99% D), and NaOD (99% D).

Spectroscopic Measurements. UV-vis spectra were measured on a Hewlett-Packard 8452A diode-array spectrophotometer. NMR spectra were measured on a JEOL JNM-LA500 spectrometer or a Bruker UltraShield 400 MHz spectrometer.

Photochemical reduction of $[\text{Ru}(\text{bpy})_2(\text{pbn})](\text{PF}_6)_2$ was conducted in either $\text{CH}_3\text{CN}/\text{Et}_3\text{N}$ (4:1 v/v) under vacuum or N_2 -bubbled DMF/TEOA (4:1 v/v). The solution was irradiated either with monochromated light (± 6 nm) or with light through a cutoff filter using a 75 or 150 W lamp. The quantum yield was measured with a 1.0×10^{-4} M $[\text{Ru}(\text{bpy})_2(\text{pbn})]^{2+}$ solution in $\text{CH}_3\text{CN}/\text{TEA}$ (v/v = 3.5) at 355 ± 6 nm using a potassium ferrioxalate actinometry.¹² Solutions of the reduced species were prepared under vacuum by sodium amalgam (Na-Hg, 0.5% Na in Hg) in CH_3CN in sealed glassware equipped with an optical cell.

Flash Photolysis Measurements. Transient absorption spectra were measured with a home-built TA setup. The second harmonic of a Continuum Surelite I YAG:Nd³⁺ laser (532 nm) was used as an excitation source. The laser was operated in pulsed mode with a repetition rate of 10 Hz and 2 mJ per pulse. A 75 W Xe arc lamp was used in pulsed mode at 10 Hz as a source of probe light. A Stanford Research DG 535 delay/pulse generator was used to synchronize the laser, the pulsed Xe lamp, and an HP 54510A oscilloscope (250 MHz, 1 GSa/s). The probe beam was focused

on the sample cell and overlapped with the laser beam in collinear fashion. After passing through the sample, the probe light was focused on the slits of an ISA monochromator, and the monochromatic light was passed to a Hamamatsu R955 PMT. The PMT anode current was measured and digitized with an HP oscilloscope. A home-developed LabView-based code was used to control all the components of the transient absorption setup as well as the acquisition and processing of transient signals.

A sample solution was placed into a vacuum-tight quartz cell (1 cm path) and degassed with three freeze-pump-thaw cycles. Transient spectra were acquired in the spectral range between 390 and 800 nm every 5 nm with at least 16 averages per kinetic trace. The photodecomposition of the starting material during experiments was less than 3% as determined by UV-vis spectroscopy.

Electrochemical Measurements. Electrochemical measurements of redox reactions of $[\text{Ru}(\text{bpy})_2(\text{pbn})]^{2+}$ were conducted with a BAS 100b electrochemical analyzer from Bioanalytical Systems. Electrochemical experiments were carried out using solutions of $[\text{Ru}(\text{bpy})_2(\text{pbn})]^{2+}$ (1 mM) in water containing 10 vol % of acetonitrile and 100 mM sodium triflate as an electrolyte. The acetonitrile was added to increase the solubility of $[\text{Ru}(\text{bpy})_2(\text{pbn})]^{2+}$. Sodium phosphate (5 mM) was used as a buffer between pH 3 and 10. A stationary mercury drop electrode (SMDE), a saturated calomel electrode (SCE), and a platinum wire were used as a working electrode, a reference electrode, and a counter electrode, respectively, for these measurements in aqueous solutions. Electrochemical measurements in acetonitrile were conducted with 1 mM solution of $[\text{Ru}(\text{bpy})_2(\text{pbn})]^{2+}$ in the presence of 100 mM tetrabutylammonium hexafluorophosphate. A glassy carbon electrode (GCE) was used as a working electrode.

Pulse Radiolysis. Pulse radiolysis studies were carried out using the BNL 2 MeV van de Graaff accelerator using electron pulses (pulse width of 40–500 ns) that led to irradiation doses of 100–1000 rad (ca. 0.5–5 μM primary radicals) generated in solution. A thiocyanate solution (0.01 M KSCN, 0.026 M N_2O) was used for dosimetry taking $G((\text{SCN})_2^{\cdot-}) = 6.13$ (G = number of species formed per 100 eV of energy absorbed by the solution) and $\epsilon_{472\text{nm}} = 7590 \pm 230$. The optical path of the cell was 2 cm. All measurements were carried out in 10 mM phosphate buffer, 10 mM sodium formate, and 20–80 μM $[\text{Ru}(\text{bpy})_2(\text{pbn})]^{2+}$ at 25 °C. Under these conditions, the conversion of the primary radicals to the carbon dioxide anion radical was complete by the first microsecond. Quoted rate constants have an error of ca. 15%. All rates measured in the pulse radiolysis studies are averages of at least three measurements. The pH of the solution was adjusted by addition of NaOH or H_2SO_4 .

Radiolysis of aqueous solutions produces $\cdot\text{OH}$, e_{aq}^- , and H^\cdot with G values of 2.7, 2.6 and 0.6, respectively ($\text{H}_2\text{O} \xrightarrow{\text{radiolysis}} \cdot\text{OH}, e_{\text{aq}}^-, \text{H}^\cdot, \text{H}_2, \text{H}_2\text{O}_2$).¹³ In nitrous-oxide-saturated solution, the hydrated electron is converted to OH^\cdot ($e_{\text{aq}}^- + \text{N}_2\text{O} + \text{H}_2\text{O} \rightarrow \text{OH}^\cdot + \text{OH}^- + \text{N}_2$). Radiolysis of a nitrous-oxide-saturated aqueous solution containing HCO_2^- leads to exclusive production of the carbon dioxide anion radical $\text{CO}_2^{\cdot-}$ since both OH^\cdot and H^\cdot react with HCO_2^- ($\text{OH}^\cdot/\text{H}^\cdot + \text{HCO}_2^- \rightarrow \text{H}_2\text{O}/\text{H}_2 + \text{CO}_2^{\cdot-}$). $\text{CO}_2^{\cdot-}$ is a strong reducing agent ($E = -1.90$ V)¹⁴ that undergoes protonation only under very acidic conditions ($\text{p}K_{\text{a}} = -0.2$).¹⁵

⁶⁰Co Gamma Radiolysis. Steady-state radiolysis studies were carried out using the BNL 850 Ci ⁶⁰Co γ -ray source. The chemistry that ensues is identical to that in pulse radiolysis since, in water,

(11) Riddick, J. A.; Bunger, W. B.; Sakano, T. K. *Organic Solvents, Physical Properties and Methods of Purification*, 4th ed.; Wiley: New York, 1986.

(12) Kuhn, H. J.; Braslavsky, S. E.; Schmidt, R. *Pure Appl. Chem.* **1989**, *61*, 187–210.

(13) Buxton, G. V.; Greenstock, C. L.; Helman, W. P.; Ross, A. B. *J. Phys. Chem. Ref. Data* **1988**, *17*, 513–886.

(14) Schwarz, H. A.; Dodson, R. W. *J. Phys. Chem.* **1989**, *93*, 409–414.

(15) Kawanishi, Y.; Kitamura, N.; Tazuke, S. *Inorg. Chem.* **1989**, *28*, 2968–2975.

both γ -rays and electrons produce the same yield of primary species. Here, a continuous flux of radicals produced is at a low steady-state concentration, with a production rate of ca. $0.5 \mu\text{M CO}_2^{\cdot-}/\text{s}$ in N_2O -saturated solution containing HCO_2^- .

DFT Calculations. Gas-phase DFT calculations on $[\text{Ru}(\text{bpy})_2(\text{pbn})]^{2+}$ were carried out using the hybrid B3LYP method^{16–18} and the Hay–Wadt VDZ ($n+1$) ECP (LANL2DZ ECP) basis set^{19,20} for Ru and the 6-31G** (5d) basis set^{21–23} for H, C, and N. Geometry optimizations and frequency analyses were performed using the Gaussian 03 package of programs.²⁴ Time-dependent B3LYP calculations were carried out with the Gaussian 03 program in order to predict the UV–vis spectra of the various species. The effect of solvation by acetonitrile on the UV–vis spectra of several species was carried out by reoptimizing the geometry and performing the TD-B3LYP calculation while employing a polarizable continuum model (PCM) of the solvent using united-atom, Hartree–Fock (UAHF) radii.

Results

Ground- and Excited-State Properties of $[\text{Ru}(\text{bpy})_2(\text{pbn})]^{2+}$. An aqueous solution of the $[\text{Ru}(\text{bpy})_2(\text{pbn})]^{2+}$ complex at neutral pH possesses a UV–vis absorption spectrum (Figure 1) typical for mixed-ligand complexes with two MLCT transitions centered around 530 nm ($d-\pi_{\text{pbn}}^*$) and 440 nm ($d-\pi_{\text{bpy}}^*$) and $\pi-\pi^*$ transitions of the ligands at 380 nm (pbn) and 290 nm (bpy and pbn).

We previously investigated the acid–base properties of $[\text{Ru}(\text{bpy})_2(\text{pbn})]^{2+}$ in water and found that the N atom (N5) of the naphthyridine moiety can be readily protonated to form $[\text{Ru}(\text{bpy})_2(\text{pbnH})]^{3+}$ ($\text{p}K_a = 1.7$) with a decrease in the absorption at 533 nm and the appearance of an absorption at 610 nm.¹⁰ The absorption band at 533 nm has been assigned as an MLCT band associated with the pbn ligand based on TD-DFT calculations.¹⁰ The spectral change accompanying the formation of $[\text{Ru}(\text{bpy})_2(\text{pbnH})]^{3+}$ from $[\text{Ru}(\text{bpy})_2(\text{pbn})]^{2+}$ agrees with this assignment.

Reduction of $[\text{Ru}(\text{bpy})_2(\text{pbn})]^{2+}$ in CH_3CN shows reversible waves at 0.66, -0.72 , -1.34 , and -1.62 V versus SCE,

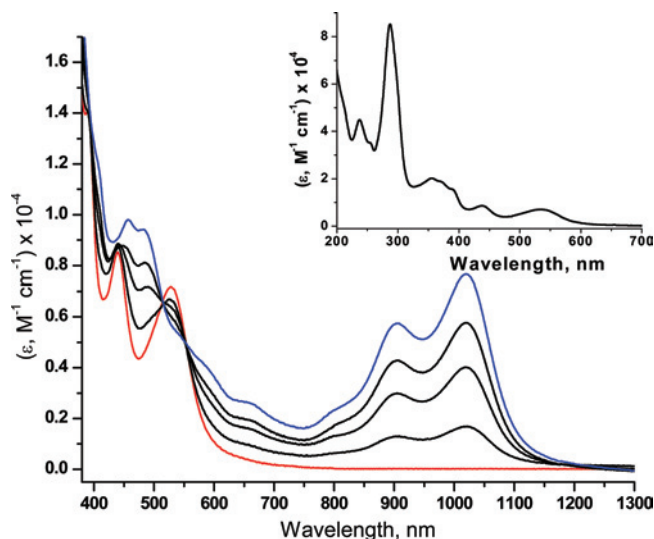


Figure 1. Stepwise reduction of $[\text{Ru}(\text{bpy})_2(\text{pbn})]^{2+}$ (red) by Na–Hg in CH_3CN to form $[\text{Ru}(\text{bpy})_2(\text{pbn}^{\cdot-})]^+$ (blue). Inset: UV–vis spectrum of $[\text{Ru}(\text{bpy})_2(\text{pbn})]^{2+}$ in aqueous solution at pH 7.0.

which can be assigned to $\text{Ru}^{3+}/\text{Ru}^{2+}$, $\text{pbn}/\text{pbn}^{\cdot-}$, $(\text{bpy})_2/(\text{bpy}, \text{bpy}^{\cdot-})$, and $(\text{bpy}, \text{bpy}^{\cdot-})/(\text{bpy}^{\cdot-})_2$, respectively. Reduction of $[\text{Ru}(\text{bpy})_2(\text{pbn})]^{2+}$ in aqueous solutions yields three quasi-reversible redox waves with two pH-independent potentials around -1.60 and -1.40 V, while the potential of the third wave varies between -0.35 and -0.80 V over pH 2–11. The slope of the pH-dependent wave was 59 mV/pH, which clearly indicates the proton-coupled nature of this redox reaction to produce the neutral ligand radical complex, $[\text{Ru}(\text{bpy})_2(\text{pbnH}^{\cdot})]^{2+}$. The $\text{p}K_a$ obtained by acid titration agreed well with the value obtained by cyclic voltammetry.

UV–vis–NIR spectral changes during the one-electron reduction of $[\text{Ru}(\text{bpy})_2(\text{pbn})]^{2+}$ in CH_3CN are shown in Figure 1. With the decrease in intensity of bands at 288 and 526 nm, new bands appear at 342, 366, 404sh, 456, 480, 600sh, 650sh, 800sh, 900, and 1020 nm. This spectral change is indicative of the formation of the pbn anion radical but not the bpy anion radical. These experimental observations are also consistent with the spectral change predicted by TD-B3LYP calculations employing a PCM treatment of an acetonitrile solution except that all absorption bands are blue-shifted (Figure S1, see Supporting Information).

The 532 nm excitation of the $[\text{Ru}(\text{bpy})_2(\text{pbn})]^{2+}$ complex into its MLCT ($d-\pi_{\text{pbn}}^*$) band yields a transient spectrum (Figure 2) with a broad band between 560 and 800 nm centered around 700 nm, a narrow transient band around 400 nm, and the bleaching of the ground-state absorption around 450 and 550 nm. The lifetimes of the excited state in acetonitrile and water (pH > 5) were about 140 and 30 ns, respectively. The lifetime of the transient was strongly pH-dependent (Figure 3) in the region near the $\text{p}K_a$ ($=1.7$) of the $[\text{Ru}(\text{bpy})_2(\text{pbnH})]^{3+}$ complex and became shorter than the time resolution of the transient absorption setup below pH 2.

The presence of 1,4-diazabicyclo[2.2.2]octane (DABCO) causes dramatic changes in the transient spectrum (Figure 4B) due to the reductive quenching of the excited state of $[\text{Ru}(\text{bpy})_2(\text{pbn})]^{2+}$. We compared this spectrum with that

- (16) Becke, A. D. *Phys. Rev. A* **1988**, *38*, 3098–3100.
- (17) Lee, C. T.; Yang, W. T.; Parr, R. G. *Phys. Rev. B* **1988**, *37*, 785–789.
- (18) Miehlich, B.; Savin, A.; Stoll, H.; Preuss, H. *Chem. Phys. Lett.* **1989**, *157*, 200–206.
- (19) Hay, P. J.; Wadt, W. R. *J. Chem. Phys.* **1985**, *82*, 270–283.
- (20) Wadt, W. R.; Hay, P. J. *J. Chem. Phys.* **1985**, *82*, 284–298.
- (21) Ditchfield, R.; Hehre, W. J.; Pople, J. A. *J. Chem. Phys.* **1971**, *54*, 724–728.
- (22) Harihara, P. C.; Pople, J. A. *Theor. Chim. Acta* **1973**, *28*, 213–222.
- (23) Hehre, W. J.; Ditchfield, R.; Pople, J. A. *J. Chem. Phys.* **1972**, *56*, 2257–2261.
- (24) Frisch, M. J.; Trucks, G. W.; Schlegel, H. B.; Scuseria, G. E.; Robb, M. A.; Cheeseman, J. R.; Montgomery, J. A., Jr.; Vreven, T.; Kudin, K. N.; Burant, J. C.; Millam, J. M.; Iyengar, S. S.; Tomasi, J.; Barone, V.; Mennucci, B.; Cossi, M.; Scalmani, G.; Rega, N.; Petersson, G. A.; Nakatsuji, H.; Hada, M.; Ehara, M.; Toyota, K.; Fukuda, R.; Hasegawa, J.; Ishida, M.; Nakajima, T.; Honda, Y.; Kitao, O.; Nakai, H.; Klene, M.; Li, X.; Knox, J. E.; Hratchian, H. P.; Cross, J. B.; Bakken, V.; Adamo, C.; Jaramillo, J.; Gomperts, R.; Stratmann, R. E.; Yazyev, O.; Austin, A. J.; Cammi, R.; Pomelli, C.; Ochterski, J. W.; Ayala, P. Y.; Morokuma, K.; Voth, G. A.; Salvador, P.; Dannenberg, J. J.; Zakrzewski, V. G.; Dapprich, S.; Daniels, A. D.; Strain, M. C.; Farkas, O.; Malick, D. K.; Rabuck, A. D.; Raghavachari, K.; Foresman, J. B.; Ortiz, J. V.; Cui, Q.; Baboul, A. G.; Clifford, S.; Cioslowski, J.; Stefanov, B. B.; Liu, G.; Liashenko, A.; Piskorz, P.; Komaromi, I.; Martin, R. L.; Fox, D. J.; Keith, T.; Al-Laham, M. A.; Peng, C. Y.; Nanayakkara, A.; Challacombe, M.; Gill, P. M. W.; Johnson, B.; Chen, W.; Wong, M. W.; Gonzalez, C.; Pople, J. A. *Gaussian 03*, revision B.04; Gaussian, Inc.: Wallingford, CT, 2004.

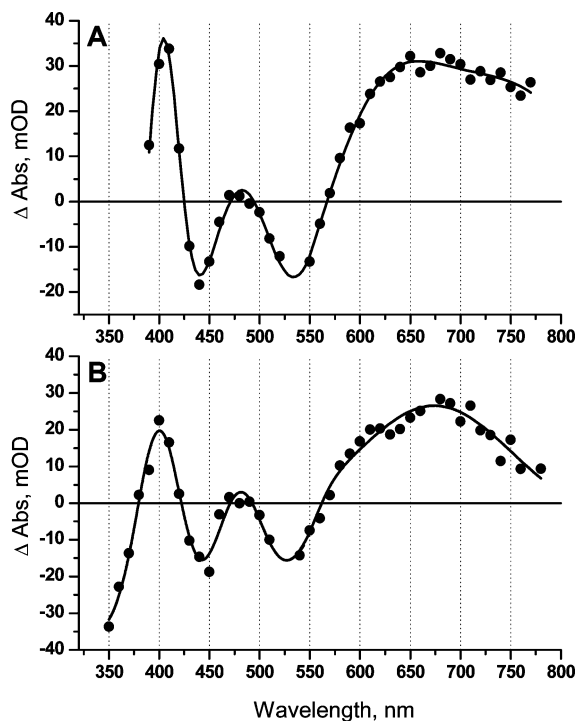


Figure 2. Transient absorption spectrum measured after 532 nm excitation of $[\text{Ru}(\text{bpy})_2(\text{pbn})]^{2+}$ in acetonitrile after 90 ns delay (A) and in water at pH 11 after 50 ns delay (B). “mOD” denotes milli (10^{-3}) optical density.

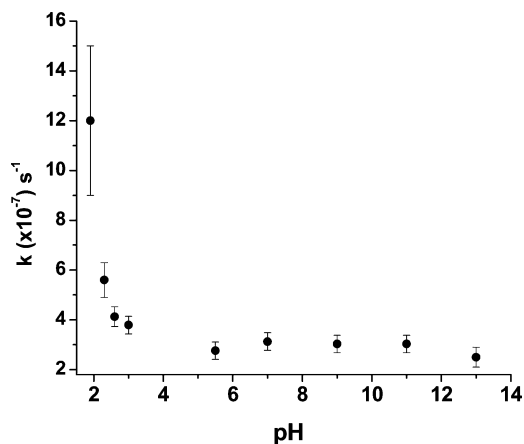


Figure 3. Kinetic behavior of the excited-state decay measured at 670 nm in water at various $[\text{H}^+]$.

obtained by Na–Hg one-electron reduction of $[\text{Ru}(\text{bpy})_2(\text{pbn})]^{2+}$ in CH_3CN (Figure 4A), for which the difference spectrum contains a broad and rather flat peak at 474 nm. The broad difference peak arises from the subtraction of the spectrum of $[\text{Ru}(\text{bpy})_2(\text{pbn})]^{2+}$ that has λ_{min} at 480 nm from the spectrum of $[\text{Ru}(\text{bpy})_2(\text{pbn}^{\cdot-})]^+$ that contains two closely located peaks at 456 and 480 nm (see Figure 1). One of the most noticeable differences between Figure 4A and 4B is an intense absorption centered at 480 nm that is due to the spectral overlap of a characteristic absorption of the DABCO radical cation species^{25,26} with the peak of the Ru species. Overall, the difference spectrum obtained by the reductive quenching is consistent with that obtained by Na–Hg reduction.

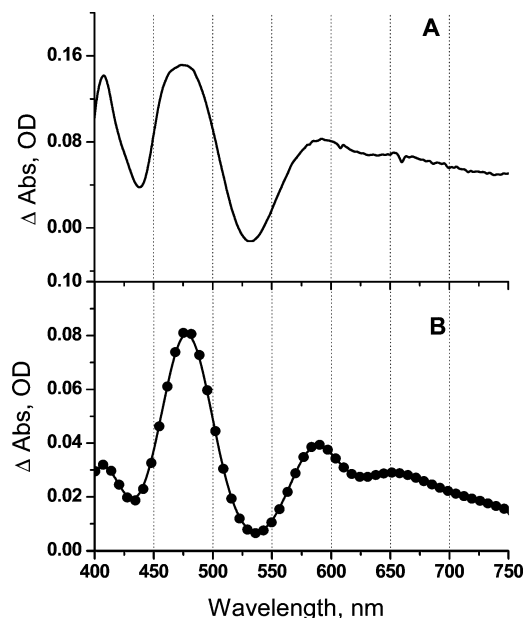


Figure 4. Difference spectrum obtained after reduction of $[\text{Ru}(\text{bpy})_2(\text{pbn})]^{2+}$ with one-electron reduction by sodium amalgam in CH_3CN (A) and transient absorption spectrum measured 3 μs after 532 nm excitation of acetonitrile solution of $[\text{Ru}(\text{bpy})_2(\text{pbn})]^{2+}$ in the presence of DABCO (B).

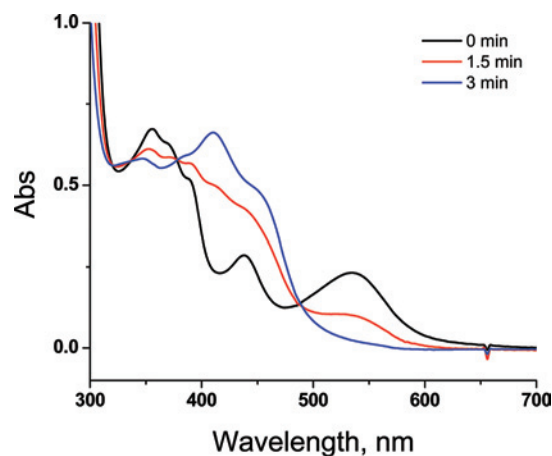


Figure 5. Reduction of $[\text{Ru}(\text{bpy})_2(\text{pbn})]^{2+}$ with e_{aq}^- and $\text{CO}_2^{\cdot-}$ at pH = 8.9.

The bimolecular rate constant of quenching of the $[\text{Ru}(\text{bpy})_2(\text{pbn})]^{2+}$ excited state by DABCO in acetonitrile was found to be close to the diffusion-controlled limit with the value of $1.1 \times 10^9 \text{ M}^{-1} \text{ s}^{-1}$ (Figure S2).

Continuous Radiolysis. Upon γ -irradiation (^{60}Co source) of an Ar- or N_2O -saturated $[\text{Ru}(\text{bpy})_2(\text{pbn})]^{2+}$ aqueous solution (ca. 40 μM) containing 10 mM NaHCO_2 , the e_{aq}^- and/or $\text{CO}_2^{\cdot-}$ are produced in situ and continually reduce the starting material. Loss of the starting ruthenium compound was accomplished in 3 min, the time required to produce the equivalent of 90 μM of reducing radical (Figure 5). The final spectrum is identical to that of $[\text{Ru}(\text{bpy})_2(\text{pbnHH})]^{2+}$ prepared by $\text{Na}_2\text{S}_2\text{O}_4$ or photoirradiation with triethylamine.¹⁰ This species has been fully characterized by

(25) Shida, T.; Nosaka, Y.; Kato, T. *J. Phys. Chem.* **1978**, *82*, 695–698.
 (26) Balakrishnan, G.; Keszthelyi, T.; Wilbrandt, R.; Zwier, J. M.; Brouwer, A. M.; Buma, W. J. *J. Phys. Chem. A* **2000**, *104*, 1834–1841.

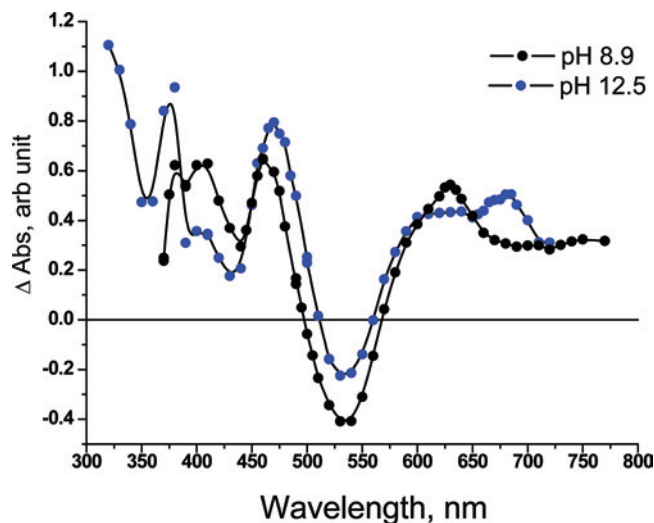
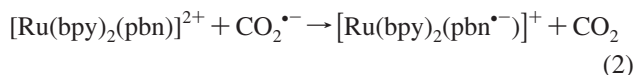
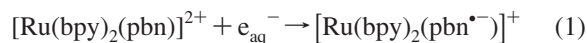


Figure 6. Two UV-vis difference spectra measured immediately after exposure of $[\text{Ru}(\text{bpy})_2(\text{pbn})]^{2+}$ aqueous solutions to transient concentrations of $\text{CO}_2^{\bullet-}$ radical at different pH values (8.9 and 12.5). The solutions were buffered with 10 mM phosphate buffer.

high-resolution electrospray mass spectrometry and a single-crystal X-ray diffraction study.¹⁰

Pulse Radiolysis. The exposure of $[\text{Ru}(\text{bpy})_2(\text{pbn})]^{2+}$ in aqueous solutions to transient concentrations of e_{aq}^- or $\text{CO}_2^{\bullet-}$ led to the formation of a single transient absorption spectrum independent of the type of reducing species at pH 10.0. The reactions between $e_{\text{aq}}^-/\text{CO}_2^{\bullet-}$ and $[\text{Ru}(\text{bpy})_2(\text{pbn})]^{2+}$ (eqs 1 and 2) were monitored by the decay of the band due to the absorption of e_{aq}^- at 680 nm and the formation of the reduced species $[\text{Ru}(\text{bpy})_2(\text{pbn})]^{2+}$ at 470 nm. The growth of the 470 nm signal was fitted with a biexponential kinetic model, with a fast component corresponding to the reaction with the solvated electron and a slow component corresponding to the reaction with $\text{CO}_2^{\bullet-}$ (see Figure S3). The bimolecular rate constants for reactions of e_{aq}^- and $\text{CO}_2^{\bullet-}$ with $[\text{Ru}(\text{bpy})_2(\text{pbn})]^{2+}$ were determined by varying (10–80 μM) the amount of the starting complex under conditions that are pseudo-first-order in e_{aq}^- and $\text{CO}_2^{\bullet-}$ at pH 10. The linear plots of the observed rates for the formation of $[\text{Ru}(\text{bpy})_2(\text{pbn}^{\bullet-})]^+$ with e_{aq}^- and $\text{CO}_2^{\bullet-}$ as a function of the $[\text{Ru}(\text{bpy})_2(\text{pbn})]^{2+}$ concentration give $k_1 = 3.0 \times 10^{10} \text{ M}^{-1} \text{ s}^{-1}$ and $k_2 = 4.6 \times 10^9 \text{ M}^{-1} \text{ s}^{-1}$, respectively (Figures S4 and S5).



While the formation of a single transient absorption spectrum upon pulse radiolysis is independent of the type of reducing species (i.e., e_{aq}^- or $\text{CO}_2^{\bullet-}$) at pH 10 as described above, the observed difference spectra varied significantly in the pH range from 8 to 12.5 (Figure 6). The observed difference spectra (Figure 6) can be corrected for the loss of parent species, assuming the 1:1 stoichiometry given in reactions 1 and 2, the absorption spectra of transient species at two different pH values can be calculated (Figure 7). The UV-vis spectrum of the initially observed species at pH 12.5

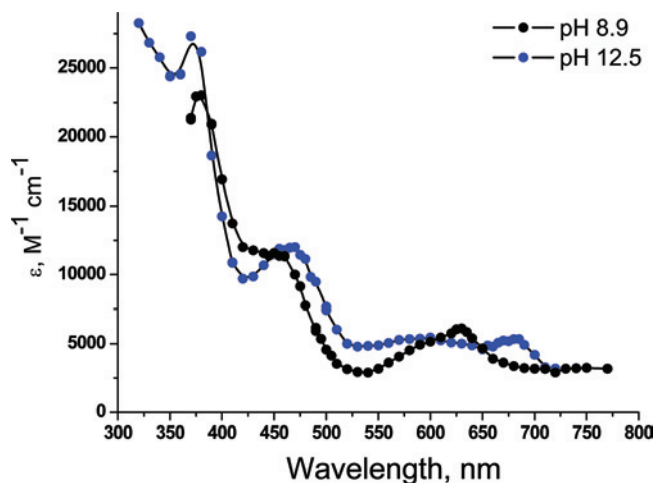


Figure 7. Two UV-vis spectra measured immediately after exposure of $[\text{Ru}(\text{bpy})_2(\text{pbn})]^{2+}$ aqueous solutions to transient concentrations of $\text{CO}_2^{\bullet-}$ radical at different pH values (8.9 and 12.5), corrected for parent compound loss assuming stoichiometric loss of parent compound and generation of the transient species. The solutions were buffered with 10 mM phosphate buffer.

Table 1. Relative Electronic Energies (in kcal mol⁻¹) of $\text{Ru}(\text{bpy})_2(\text{pbn})$ Species in the Gas Phase and in Acetonitrile Solution

species	gas phase	acetonitrile solution
$[\text{Ru}(\text{bpy})_2(\text{pbn})]^{2+}$	0.0	0.0
$[\text{Ru}(\text{bpy})_2(\text{pbn}^{\bullet-})]^+$	-157.9	-89.0
$[\text{Ru}(\text{bpy})_2(\text{pbnH}^{\bullet})]^{2+}$	-385.3	-383.6
$[\text{Ru}(\text{bpy})_2(\text{pbnHH})]^{2+}$	-769.4	-768.8
ΔE (disproportionation)	1.1	-1.6

exhibits absorption bands around 470, 600, and 680 nm and is consistent with that of the one-electron-reduced species produced by Na-Hg reduction or reductive quenching of the excited state of $[\text{Ru}(\text{bpy})_2(\text{pbn})]^{2+}$. The minor spectral differences may arise due to different solvents used in pulse radiolysis and chemical reduction experiments. Lowering the pH to 8.9 causes a slight blue shift (10 nm) of the 470 band and a significant blue shift (50 nm) of the 680 nm absorption (Figure 7).

Theoretical Calculations of Electronic Energies. We have carried out electronic energy calculations that optimized the geometry of the various $\text{Ru}(\text{bpy})_2(\text{pbn})$ species in the gas phase and in a PCM treatment of acetonitrile. In the PCM calculations, united-atom Hartree-Fock radii were used to define the cavity around the solute molecule. The convention used here is to assign the electronic energy of both the free, gas-phase electron, and proton to be zero. We assume that the gas-phase species are formed first (e.g., by the addition of free electrons and/or protons to $[\text{Ru}(\text{bpy})_2(\text{pbn}^{\bullet-})]^+$), and that the resulting species are then placed into acetonitrile solution. The electronic energy change for the disproportionation reaction of $[\text{Ru}(\text{bpy})_2(\text{pbnH}^{\bullet})]^{2+}$ is independent of this convention because the same number of electrons and protons are present in both reactants and products. The results indicate that the disproportionation reaction is slightly exoergic ($\Delta E = -1.6 \text{ kcal mol}^{-1}$) in acetonitrile solution (Table 1). It is also evident that the smaller solvation energy of the 1+ $[\text{Ru}(\text{bpy})_2(\text{pbn}^{\bullet-})]^+$ ion (compared to the other 2+ ions) destabilizes that species relative to $[\text{Ru}(\text{bpy})_2-$

(pbn)]²⁺ in acetonitrile solution, thereby making it a stronger proton acceptor to form [Ru(bpy)₂(pbnH⁺)]²⁺.

Discussion

Excited-State photochemistry. An optical excitation into the MLCT transition at 530 nm ($d-\pi_{\text{pbn}}^*$) produces a transient absorption spectrum of the [Ru(bpy)₂(pbn)]²⁺ excited state that decays monoexponentially with a rate around $3 \times 10^7 \text{ s}^{-1}$ in water (pH 5–13). The red shift of the absorption band in the excited state as compared to the that in the ground state (Figure 2) is consistent with reduction of one of the ligands and oxidation of the metal center.²⁷ The considerable difference between the excited-state absorption spectra of [Ru(bpy)₃]²⁺²⁸ and [Ru(bpy)₂(pbn)]²⁺ indicates that the electron density is predominantly transferred to naphthyridine, and not to the bpy ligand, as a result of photoexcitation.

The protonated *[Ru(bpy)₂(pbn)]²⁺ is expected to be a weaker acid than the protonated ground-state species due to its MLCT nature (i.e., close to [Ru^{III}(bpy)₂(pbn^{•-})]²⁺). The excited-state spectra measured in water (in the pH range from 5 to 13) and acetonitrile (where the protonation of an excited state is impossible) are very similar, indicating the same origin of the observed species (Figure 2). The excited-state lifetime in water was about 5 times shorter than that in acetonitrile solutions. Minor differences in lifetimes and absorption spectra may be explained in terms of different solvation of *[Ru(bpy)₂(pbn)]²⁺ and [Ru(bpy)₂(pbn)]²⁺ by water and acetonitrile. In some ruthenium complexes containing bpz or bpm (where bpz = 2,2'-bipyrazine and bpm = 2,2'-bipyrimidine) ligands, significantly shorter lifetimes and lower emission intensities were observed together with spectral shifts when the excited states are protonated.²⁹ In these systems, since luminescence from the protonated excited state is observable, the lifetime and $\text{p}K_{\text{a}}^*$ (of the protonated excited-state species) were directly determined. The relationship $\text{p}K_{\text{a}}^* - \text{p}K_{\text{a}} = 4.8$ has been reported.²⁹ Assuming a similar relation, the $\text{p}K_{\text{a}}^*$ of *[Ru(bpy)₂(pbnH)]³⁺ (i.e., the N5 protonated species) should be observed around 6; however, we did not observe any significant change in the excited-state lifetime in this region, and therefore, we could not determine the $\text{p}K_{\text{a}}^*$. The lifetime of *[Ru(bpy)₂(pbn)]²⁺ is relatively short ($k_{\text{obs}} = 3 \times 10^7 \text{ s}^{-1}$); therefore, the protonation by H⁺ should not take place in the excited state assuming the rate of protonation is almost diffusion-limited ($\sim 3 \times 10^{10} \text{ M}^{-1} \text{ s}^{-1}$) and [H⁺] = 10⁻⁶. Even if water acts as a proton source (see the Mechanism of Formation of [Ru(bpy)₂(pbnHH)]²⁺ section below), the excited-state lifetime is too short for effective protonation. The pH-dependent decay of the excited state (Figure 3) looks similar to the pH titration curve of the ground-state complex, consistent with the significantly shorter lifetime (a factor of 3–4) of the

protonated excited-state species. We believe equilibrium between the nonprotonated and protonated excited-state species is not established within the lifetime of the excited state, even though the change in electron density in the naphthyridine ligand upon electronic excitation is sufficient to substantially increase the basicity in the excited state compared to the ground state. Using the triplet excited state as a model of the electronic configuration of the photoexcited singlet state, B3LYP calculations (Figure S6) predict that about one-sixth of the net change in spin density between the ground and triplet excited states of [Ru(bpy)₂(pbn)]²⁺ contribute to increased electron density on the nitrogen atom N5 of the pbn ligand.

The excited state of [Ru(bpy)₂(pbn)]²⁺ can be successfully quenched by electron donors (e.g., DABCO) to produce a radical anion species. Though the spectrum is dominated by absorption of the DABCO radical cation around 475 nm, the absorption at longer wavelengths is similar to the spectrum of [Ru(bpy)₂(pbn^{•-})]⁺ obtained by Na–Hg reduction (Figure 4). The signals attributed to absorptions of [Ru(bpy)₂(pbn^{•-})]⁺ and DABCO^{•+} decayed to fully recover the starting materials. The quenching of the excited state of [Ru(bpy)₂(pbn)]²⁺ with triethanolamine (TEOA) or triethylamine (TEA) in continuous photolysis experiments ($\lambda > 300 \text{ nm}$) leads to the formation of [Ru(bpy)₂(pbnHH)]²⁺,¹⁰ presumably following the same pathway as observed by pulse radiolysis.

Mechanism of Formation of [Ru(bpy)₂(pbnHH)]²⁺. The reduction of [Ru(bpy)₂(pbn)]²⁺ by $\text{e}_{\text{aq}}^-/\text{CO}_2^{\bullet-}$ leads to the formation of the reduced species [Ru(bpy)₂(pbn^{•-})]⁺ that exhibits a distinctive UV–vis spectrum that is different from that of [Ru(bpy)₃]⁺,³⁰ indicating that it is predominantly the pbn ligand that is reduced. The rate constant of the reaction between e_{aq}^- and [Ru(bpy)₂(pbn)]²⁺ ($3.0 \times 10^{10} \text{ M}^{-1} \text{ s}^{-1}$; pH = 10) is diffusion-controlled and is comparable to those reported for reactions of ruthenium polypyridine complexes with e_{aq}^- (3.1×10^{10} to $8.2 \times 10^{10} \text{ M}^{-1} \text{ s}^{-1}$).^{31–34} The rate constant of the [Ru(bpy)₂(pbn)]²⁺ reduction by $\text{CO}_2^{\bullet-}$ is also high ($4.6 \times 10^9 \text{ M}^{-1} \text{ s}^{-1}$; pH = 10) and similar to the rate constant of the reduction of ruthenium complexes containing bpz and bpm ligands by $\text{CO}_2^{\bullet-}$ (1.3×10^{10} to $4.7 \times 10^9 \text{ M}^{-1} \text{ s}^{-1}$),^{35,36} but yet 2 orders of magnitude higher than that for the reduction of [Ru(bpy)₃]²⁺ by $\text{CO}_2^{\bullet-}$ ($6.0 \times 10^7 \text{ M}^{-1} \text{ s}^{-1}$).³⁶ This difference in reduction rates also suggests that the pbn ligand rather than bpy is reduced as a result of this

(27) Amouyal, E.; Bahout, M.; Calzaferri, G. *J. Phys. Chem.* **1991**, *95*, 7641–7649.

(28) Juris, A.; Balzani, V.; Barigelli, F.; Campagna, S.; Belsler, P.; Vonzelewsky, A. *Coord. Chem. Rev.* **1988**, *84*, 85–277.

(29) Sun, H.; Hoffman, M. Z. *J. Phys. Chem.* **1993**, *97*, 5014–5018.

(30) Mulazzani, Q. G.; Emmi, S.; Fuochi, P. G.; Hoffman, M. Z.; Venturi, M. *J. Am. Chem. Soc.* **1978**, *100*, 981–983.

(31) Meisel, D.; Matheson, M. S.; Mulac, W. A.; Rabani, J. J. *Phys. Chem.* **1977**, *81*, 1449–1455.

(32) Mulazzani, Q. G.; Dangelantonio, M.; Camaioni, N.; Venturi, M. *J. Chem. Soc., Faraday Trans.* **1991**, *87*, 2179–2185.

(33) Baxendale, J.; Fiti, M. *J. Chem. Soc., Dalton Trans.* **1972**, 1995–1998.

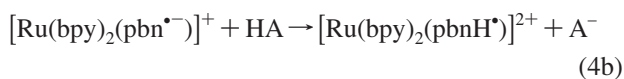
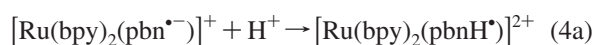
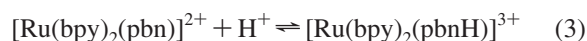
(34) Parsons, B. J.; Beaumont, P. C.; Navaratnam, S.; Harrison, W. D.; Akasheh, T. S.; Othman, M. *Inorg. Chem.* **1994**, *33*, 157–163.

(35) Venturi, M.; Mulazzani, Q. G.; Ciano, M.; Hoffman, M. Z. *Inorg. Chem.* **1986**, *25*, 4493–4498.

(36) Venturi, M.; Mulazzani, Q. G.; Dangelantonio, M.; Ciano, M.; Hoffman, M. Z. *Radiat. Phys. Chem.* **1991**, *37*, 449–456.

reaction. The rate of the reaction of $\text{CO}_2^{\bullet-}$ with the starting material was found to be almost constant between pH 3 and 11 (see Figure S7).

The observation of the pH-dependent transient absorption spectra (Figure 6) upon reduction of the $[\text{Ru}(\text{bpy})_2(\text{pbn})]^{2+}$ complex points toward the formation of the reduced species and its conjugate acid. The results of electrochemical reduction of $[\text{Ru}(\text{bpy})_2(\text{pbn})]^{2+}$ in aqueous solutions also indicate the proton-coupled nature of the redox reaction in the pH range between 2 and 11. The lowest $\text{p}K_{\text{a}}$ (ca. 2) measured in electrochemical experiments is consistent with the $\text{p}K_{\text{a}}$ of the protonated ground-state species $[\text{Ru}(\text{bpy})_2(\text{pbnH})]^{3+}$ (eq 3), while the highest (around 11) should correspond to the $\text{p}K_{\text{a}}$ of the protonated one-electron-reduced species $[\text{Ru}(\text{bpy})_2(\text{pbnH}^{\bullet})]^{2+}$ (eqs 4a or 4b)



$[\text{Ru}(\text{bpy})_2(\text{pbn}^{\bullet-})]^{+}$ is readily protonated at lower pH, yielding $[\text{Ru}(\text{bpy})_2(\text{pbnH}^{\bullet})]^{2+}$ with an absorption spectrum distinctly different from that of the one-electron-reduced species (Figure 7). Interestingly, the protonated species was formed within the time frame of the reaction between $e_{\text{aq}}^-/\text{CO}_2^{\bullet-}$ and $[\text{Ru}(\text{bpy})_2(\text{pbn})]^{2+}$ ($\sim 10 \mu\text{s}$ at $20 \mu\text{M}$ of $[\text{Ru}(\text{bpy})_2(\text{pbn})]^{2+}$) even with a low phosphate buffer concentration (ca. $2 \mu\text{M}$, see Figure S8) at pH 10. The concentration of $[\text{Ru}(\text{bpy})_2(\text{pbn})]^{2+}$ is close to the solubility limit of this species, making it impossible to accelerate formation of the initial unprotonated radical species. According to this observation, a free proton or the phosphate buffer can be excluded as a potential proton source in reaction 4a, as this would require rate constants that far exceed diffusion limits. A few systems are known in which water acts as a proton source, with rate constants of protonation as high as $10^5 \text{ M}^{-1} \text{ s}^{-1}$ for the ketoprofen (i.e., 2-[3-benzoylphenyl]propionic acid) carbanion³⁷ or $2.2 \times 10^2 \text{ M}^{-1} \text{ s}^{-1}$ for the acridine radical.³⁸ We propose that the earlier stage of transformation of $[\text{Ru}(\text{bpy})_2(\text{pbn}^{\bullet-})]^{+}$ into other species involves direct protonation of $[\text{Ru}(\text{bpy})_2(\text{pbn}^{\bullet-})]^{+}$ from water with $k_{\text{prot}} \geq 2 \times 10^3 \text{ M}^{-1} \text{ s}^{-1}$.

The blue shift of the absorption bands of the protonated one-electron-reduced species compared to its conjugate base is commonly observed in Ru complexes with ligands containing noncoordinated nitrogen atom sites available for protonation (e.g., bpz or dpp ligands).³⁹ A $\text{p}K_{\text{a}}$ value of 11.0 for the $[\text{Ru}(\text{bpy})_2(\text{pbnH}^{\bullet})]^{2+}/[\text{Ru}(\text{bpy})_2(\text{pbn}^{\bullet-})]^{+}$ equilibrium was found by measuring the pH-dependent change in the absorption spectrum (Figure 8). This $\text{p}K_{\text{a}}$ value is consistent with the one obtained in electrochemical experiments. The

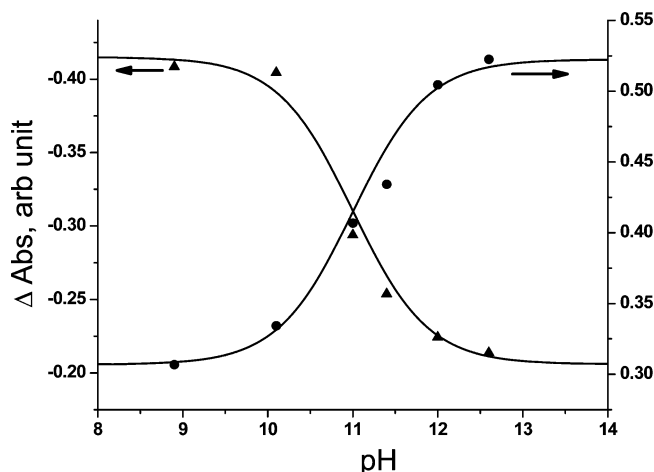


Figure 8. Titration curves obtained by plotting absorbances measured immediately after exposure of $[\text{Ru}(\text{bpy})_2(\text{pbn})]^{2+}$ aqueous solutions to transient concentrations of $\text{CO}_2^{\bullet-}$ radical versus pH at 680 nm (dots) and 530 nm (triangles). Solid line is the fit with eq 5 at $\text{p}K_{\text{a}} = 11.0$.

direct comparison of the obtained $\text{p}K_{\text{a}}$ for $[\text{Ru}(\text{bpy})_2(\text{pbnH}^{\bullet})]^{2+}$ with the one-electron reduced Ru complexes containing noncoordinated nitrogen atoms (with similar $\text{RuL}^{2+}/\text{RuL}^{+}$ redox potential) indicates that the $\text{p}K_{\text{a}}$ of $[\text{Ru}(\text{bpy})_2(\text{pbnH}^{\bullet})]^{2+}$ is substantially higher than those for complexes containing bpz and bpm ligands⁴⁰ ($\text{p}K_{\text{a}}$ around 8) and slightly higher than that of $[\text{Ru}(\text{bpy})_2(\text{dppH})]^{2+}$ (dpp = 2,3-bis(2-pyridyl)pyrazine, $\text{p}K_{\text{a}} = 10.5$ ³⁹). While several groups have reported a correlation between the reduction potential $E^\circ(\text{Ru}^{2+/+})$ and the $\text{p}K_{\text{a}}$ of the conjugate acid (i.e., the easier to be reduced, the more difficult to be protonated),^{39–42} only limited reports exist^{40,41} discussing the pH-dependent decay of the one-electron-reduced species and its conjugate acid. The final products have not been fully characterized.

$$\epsilon = \frac{\epsilon_1 + \epsilon_2 \frac{K_{\text{a}}}{[\text{H}^+]}}{1 + \frac{K_{\text{a}}}{[\text{H}^+]}} \quad (5)$$

The absorbance attributable to both $[\text{Ru}(\text{bpy})_2(\text{pbn}^{\bullet-})]^{+}$ and its conjugate acid, $[\text{Ru}(\text{bpy})_2(\text{pbnH}^{\bullet})]^{2+}$, disappeared via pH-dependent, second-order kinetics (see Figure 9 and Figure S9), consistent with the disproportionation reaction through a bimolecular process as found in the previous cases.^{40,41} Decay reaction rate constants of $[\text{Ru}(\text{bpy})_2(\text{pypm}^{\bullet-})]^{+}$ (pypm = 2-(2'-pyridyl)pyrimidine) and its conjugate acid show a low pH plateau, a maximum around pH 7 (which is 1 pH unit lower than the $\text{p}K_{\text{a}}$ value, shown in eq 6 where L = pypm), and diminishing values in the higher pH region.³⁶ From these results, the authors suggested that the $[\text{Ru}(\text{bpy})_2(\text{pypm}^{\bullet-})]^{+}$ and $[\text{Ru}(\text{bpy})_2(\text{pypmH}^{\bullet})]^{2+}$ species react

(37) Martinez, L. J.; Scaiano, J. C. *J. Am. Chem. Soc.* **1997**, *119*, 11066–11070.

(38) Jaworski, J. S.; Cembor, M. *Tetrahedron Lett.* **2000**, *41*, 7267–7270.

(39) Anderson, P. A.; Anderson, R. F.; Furue, M.; Junk, P. C.; Keene, F. R.; Patterson, B. T.; Yeomans, B. D. *Inorg. Chem.* **2000**, *39*, 2721–2728.

(40) Dangelantonio, M.; Mulazzani, Q. G.; Venturi, M.; Ciano, M.; Hoffman, M. Z. *J. Phys. Chem.* **1991**, *95*, 5121–5129.

(41) Casalboni, F.; Mulazzani, Q. G.; Clark, C. D.; Hoffman, M. Z.; Orizondo, P. L.; Perkovic, M. W.; Rillema, D. P. *Inorg. Chem.* **1997**, *36*, 2252–2257.

(42) Sun, H.; Hoffman, M. Z.; Mulazzani, Q. G. *Res. Chem. Intermed.* **1994**, *20*, 735–754.

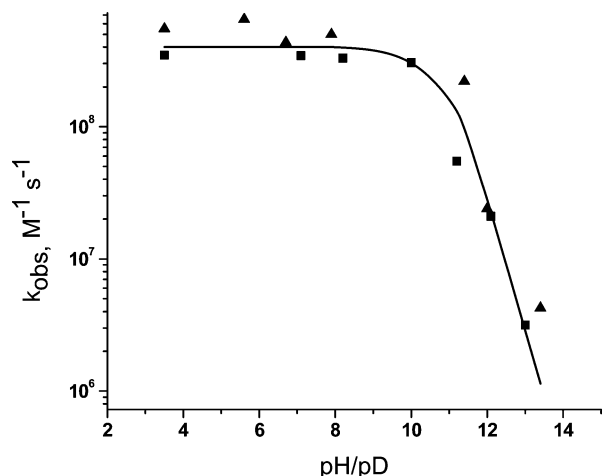
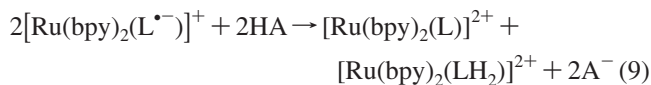
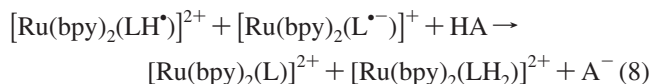
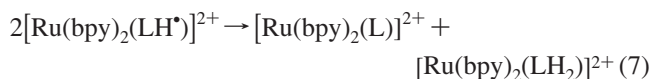


Figure 9. The pH dependence of the observed second-order rate constants for the disappearance of $[\text{Ru}(\text{bpy})_2(\text{pbnH}^*)]^{2+}$ and $[\text{Ru}(\text{bpy})_2(\text{pbnH}^*)]^{2+}$ (in H_2O = squares; in D_2O = triangles) and the fit (line) with eq 10 assuming k_9 , k_7 , and k_8 . The fit parameters are: $\text{p}K_a = 11$, $k_7 = 2.2 \times 10^8 \text{ M}^{-1} \text{ s}^{-1}$, $k_8 = 1.2 \times 10^8 \text{ M}^{-1} \text{ s}^{-1}$. There is a 10% error margin for parameters obtained from the fit.

with themselves or each other via disproportionation with different rate constants. The cross reaction (eq 8) should be faster than the self-reactions (eqs 7 and 9) due to the driving force associated with the nonsymmetric nature of the electron transfer reaction.



Then k_{obs} as a function of $[\text{H}^+]$ can be obtained from eqs 6–9 as shown in eq 10.

$$k_{\text{obs}} = \frac{2 \left[k_7 + \frac{k_8 K_a}{[\text{H}^+]} + k_9 \left(\frac{K_a}{[\text{H}^+]} \right)^2 \right]}{\left(1 + \frac{K_a}{[\text{H}^+]} \right)^2} \quad (10)$$

By fitting the data using eq 10, they obtained $k_7 = 2 \times 10^7$, $k_8 = 4 \times 10^8$, and $k_9 < 10^5 \text{ M}^{-1} \text{ s}^{-1}$ for the $[\text{Ru}(\text{bpy})_2(\text{pypm}^{\bullet-})]^{+}$ system.

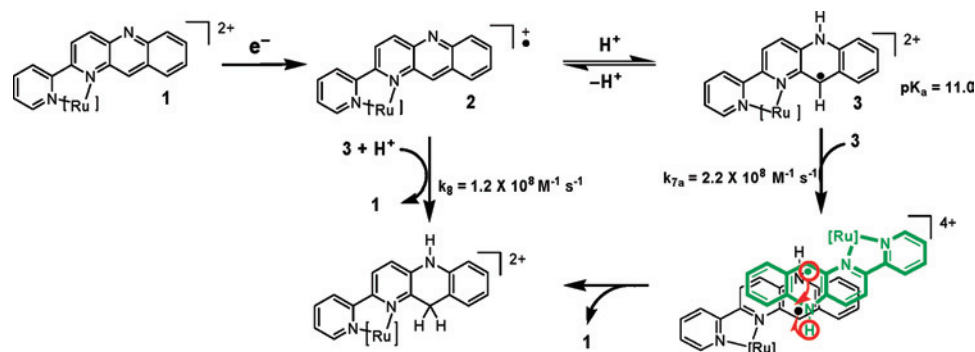
The pH-dependent rate constants for the disappearance of $[\text{Ru}(\text{bpy})_2(\text{pbnH}^*)]^{+}$ and its conjugate acid in H_2O and D_2O (Figure 9) show no significant kinetic isotope effect (KIE), suggesting protonation is not the rate-determining step. In contrast to the previous work on $[\text{Ru}(\text{bpy})_2(\text{pypm}^{\bullet-})]^{+}$, a notable increase of rate constants for the decay of $[\text{Ru}(\text{bpy})_2(\text{pbnH}^*)]^{+}$ was not observed slightly below the $\text{p}K_a$ value, suggesting that a different type of mechanism might occur instead of simple electron transfer disproportionation.

Therefore, we carefully compared the spectral changes during pulse radiolysis experiments and those during continuous γ -irradiation.

The final absorption spectrum of the product(s) in the pulse radiolysis experiments can be calculated from the observed changes in absorbance assuming a single pathway and a disproportionation mechanism with recovery of half of the starting material (eqs 7–9 and Scheme 2). In the continuous radiolysis experiments, sufficient reductant was used to completely consume all parent compound to produce $\text{Ru}(\text{bpy})_2(\text{pbnHH})^{2+}$. The calculated spectrum of $[\text{Ru}(\text{bpy})_2(\text{pbnHH})]^{2+}$ using data obtained by pulse radiolysis at pH above the $\text{p}K_a = 11.0$ matches well to the observed spectrum upon continuous exposure of $[\text{Ru}(\text{bpy})_2(\text{pbn})]^{2+}$ to $\text{CO}_2^{\bullet-}$ (Figure S10). However, the same approach did not yield a satisfactory match between the spectrum obtained in pulse radiolysis experiments measuring the bimolecular decay and spectra after continuous reduction (^{60}Co experiments) of $[\text{Ru}(\text{bpy})_2(\text{pbn})]^{2+}$ with $\text{CO}_2^{\bullet-}$ at pH below 9.0 (Figure S11). Preliminary analysis of the pulse radiolysis data indicated that no starting material was recovered after the disappearance of $[\text{Ru}(\text{bpy})_2(\text{pbnH}^*)]^{2+}$ 300 ms after a pulse. As the disappearance of $[\text{Ru}(\text{bpy})_2(\text{pbnH}^*)]^{2+}$ was clearly a second-order reaction, these observations led to the conclusion that some intermediate dinuclear species may be formed after the disproportionation step. These dinuclear species must be stable enough at room temperature to allow their observation on the pulse radiolysis time scale (ca. 300 ms). In order to confirm this hypothesis, $[\text{Ru}(\text{bpy})_2(\text{pbn})]^{2+}$ was stoichiometrically reduced at pH 8.5 with $\text{CO}_2^{\bullet-}$ at 0.2 °C (Figure 10).

Upon γ -irradiation of a N_2O -saturated $[\text{Ru}(\text{bpy})_2(\text{pbn})]^{2+}$ aqueous solution (ca. 40 μM) containing 10 mM NaHCO_2 at 0.2 °C, the complete reduction of $[\text{Ru}(\text{bpy})_2(\text{pbn})]^{2+}$ (black spectrum) by $\text{CO}_2^{\bullet-}$ led to the red spectrum in Figure 10. This intermediate spectrum at low temperature was different from that of $[\text{Ru}(\text{bpy})_2(\text{pbnHH})]^{2+}$ (see blue spectrum in Figure 5) and matched well the calculated spectrum of species in pulse radiolysis experiments (Figure S12). After warming the sample to room temperature, the absorption at 530 nm was recovered back to about half of the value of initial absorption of $[\text{Ru}(\text{bpy})_2(\text{pbn})]^{2+}$ (Figure S13). The resulting spectrum is identical to that of the equimolar mixture of the final product $[\text{Ru}(\text{bpy})_2(\text{pbnHH})]^{2+}$ and recovered starting material. Undoubtedly, this experiment validates the hypothesis that disproportionation of $[\text{Ru}(\text{bpy})_2(\text{pbnH}^*)]^{2+}$ proceeds through an intermediate dinuclear species and finally yields an equimolar mixture of $[\text{Ru}(\text{bpy})_2(\text{pbnHH})]^{2+}$ and $[\text{Ru}(\text{bpy})_2(\text{pbn})]^{2+}$. Interestingly, the disproportionation of the singly reduced species at pH above the $\text{p}K_a$ proceeds without the formation of the dinuclear intermediate, directly yielding final product and recovered starting material.

To establish a mechanistic justification of the disproportionation reaction, we calculated possible intermediates using DFT calculations of model compounds (e.g., the benzo[*b*]-1,5-naphthyridine anion radical, $\text{bn}^{\bullet-}$, and its conjugate acid, bnH^{\bullet}). The interaction between $[\text{Ru}(\text{bpy})_2(\text{pbnH}^*)]^{2+}$ and $[\text{Ru}(\text{bpy})_2(\text{pbn}^{\bullet-})]^{+}$ is difficult to model because of the

Scheme 2. The Mechanism of Formation of Final Product from the Singly Reduced Species (Water May be a Source of H⁺ at High pH)

coulombic repulsion of the two Ru(II) centers without the inclusion of counterions. We have therefore resorted to modeling the interaction without the metal centers, considering only the naphthyridine moieties. The calculations indicate that the disproportionation reaction between $\text{bn}^{\bullet-}$ and bnH^{\bullet} likely goes through a hydrogen-bonded dimer as an intermediate, followed by an electron transfer reaction from $\text{bn}^{\bullet-}$ to bnH^{\bullet} due to its driving force (see Figure S14 and Table 1 for estimation of ΔE values.). However, the disproportionation reaction between two molecules of bnH^{\bullet} goes through a π -stacking dimer, which is quite stable due to no driving force for an electron transfer reaction from a Ru unit to another Ru unit (Figure S14). These results may be applied to the disproportionation reaction for $[\text{Ru}(\text{bpy})_2(\text{pbnH}^{\bullet})]^{2+}$ and $[\text{Ru}(\text{bpy})_2(\text{pbn}^{\bullet-})]^+$.

At this point, we can speculate that formation of the dinuclear intermediate from $[\text{Ru}(\text{bpy})_2(\text{pbnH}^{\bullet})]^{2+}$ is dictated mostly by the electron density of the SOMO in the naphthyridine ligand. The analysis of spin densities in the SOMOs of $[\text{Ru}(\text{bpy})_2(\text{pbnH}^{\bullet})]^{2+}$ and its conjugate base, $[\text{Ru}(\text{bpy})_2(\text{pbn}^{\bullet-})]^+$, reveals substantial differences in unpaired electron location in the two species. In the protonated molecule, the electron density solely resides on the naphthyridine ligand with a substantial part of it on the carbon atom #11 in Figure 11 (top); however, in the nonprotonated species, the unpaired electron is localized on the bpy part of the pbn ligand and on carbon atom #11 in Figure 11 (bottom).⁴³ It can be assumed that the formation of the dinuclear

species requires intermolecular interactions involving atoms bearing high electron density (e.g., the naphthyridine ligand). This hypothesis correlates well with the fact that the dimeric intermediate was observed only in the course of reaction involving two protonated species but not in the cross reaction.

On the basis of the above discussion, a kinetic analysis of the disappearance of $[\text{Ru}(\text{bpy})_2(\text{pbnH}^{\bullet})]^{2+}$ and $[\text{Ru}(\text{bpy})_2(\text{pbn}^{\bullet-})]^+$ was performed according to eqs 6–10 except for a change in eq 7 as shown below.



The kinetic scheme, which is represented by reactions 6, 7a, 8, and 9, and k_{obs} described by eq 10 (except for replacing k_7 by k_{7a}), fits well the experimental data assuming a $\text{p}K_a$ of 11 for the $[\text{Ru}(\text{bpy})_2(\text{pbnH}^{\bullet})]^{2+}/[\text{Ru}(\text{bpy})_2(\text{pbn}^{\bullet-})]^+$ equilibrium (Figure 8). The disappearance of the singly reduced species (both protonated and nonprotonated) proceeds through two major reaction pathways with similar rates: (1) two $[\text{Ru}(\text{bpy})_2(\text{pbnH}^{\bullet})]^{2+}$ molecules forming the dimer ($k_{7a} = 2.2 \times 10^8 \text{ M}^{-1} \text{ s}^{-1}$), followed by (but not reflected in the decay kinetics of $[\text{Ru}(\text{bpy})_2(\text{LH}^{\bullet})]^{2+}$) sequential electron transfer and proton transfer disproportionation; and (2) cross reaction between the protonated and nonprotonated species ($k_8 = 1.2 \times 10^8 \text{ M}^{-1} \text{ s}^{-1}$). The obtained rate constant (k_9) of the reaction between two reduced nonprotonated molecules is negligibly small.

Generally, substantial kinetic isotope effects are observed in proton-coupled electron transfer reactions or hydrogen atom transfer.⁴⁴ The absence of an observable kinetic isotope effect in the disproportionation reaction of the one-electron-reduced forms of $[\text{Ru}(\text{bpy})_2(\text{pbn})]^{2+}$ indicates that the transfer of an electron is not likely to be coupled with proton transfer nor is a hydrogen atom transferred in the course of the reaction. In fact, at pH below 11, the observed reaction is a dimerization and not the disproportionation reaction. In the case of the reaction between $[\text{Ru}(\text{bpy})_2(\text{pbn}^{\bullet-})]^+$ and $[\text{Ru}(\text{bpy})_2(\text{pbnH}^{\bullet})]^{2+}$, it is quite possible that the formation of a hydrogen-bonded dimer occurs as shown in the case of $\text{bn}^{\bullet-}$ and bnH^{\bullet} . Even if the disproportionation reaction proceeds via the hydrogen-bonded dimer, it proceeds in a

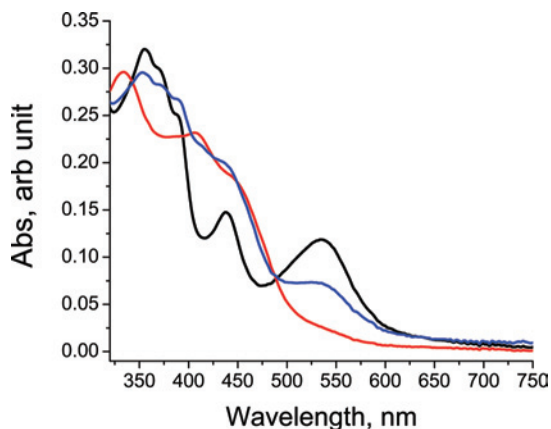


Figure 10. Reduction of $[\text{Ru}(\text{bpy})_2(\text{pbn})]^{2+}$ with $\text{CO}_2^{\bullet-}$ at pH = 8.5 and 0.2 °C. Black line: $[\text{Ru}(\text{bpy})_2(\text{pbn})]^{2+}$; red line: after reduction at 0.2 °C; blue line: after warming to 25 °C. The spectrum is identical to that of the equimolar mixture of $[\text{Ru}(\text{bpy})_2(\text{pbnH}^{\bullet})]^{2+}$ and $[\text{Ru}(\text{bpy})_2(\text{pbn})]^{2+}$.

(43) The numbering of atoms is random and does not correspond to IUPAC nomenclature.

(44) Huynh, M. H. V.; Meyer, T. J. *Proc. Natl. Acad. Sci. U.S.A.* **2004**, *101*, 13138–13141.

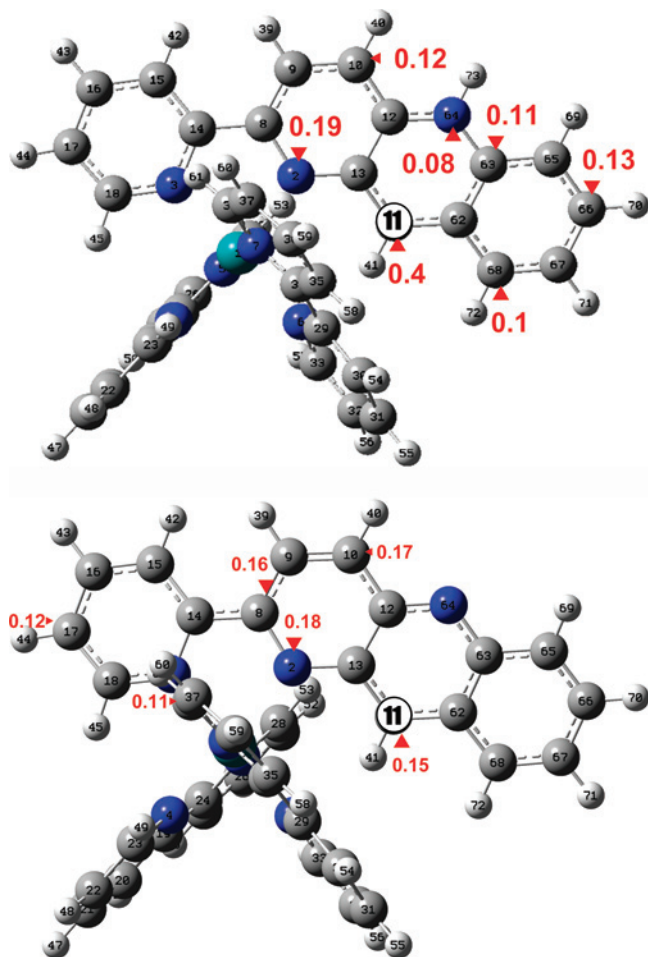


Figure 11. Spin density of an electron in the SOMO of $[\text{Ru}(\text{bpy})_2(\text{pbnH}^*)]^{2+}$ (the numbering of atoms is arbitrary and does not correspond to IUPAC nomenclature), top figure. Spin density of an electron in SOMO of $[\text{Ru}(\text{bpy})_2(\text{pbn}^{\bullet-})]^+$, bottom figure.

stepwise fashion, with electron transfer as a primary event followed by fast protonation. Despite the fact that in many cases single-step proton-coupled electron transfer is more thermodynamically favorable than stepwise reaction,⁴⁵ there is a mechanistic borderline between these two processes that is controlled by their thermodynamics.⁴⁶

Conclusions

In summary, the mechanistic pathways of formation of the NADH-like $[\text{Ru}(\text{bpy})_2(\text{pbnHH})]^{2+}$ species in aqueous medium were studied (Scheme 2). Spectra of the one-electron-reduced species $[\text{Ru}(\text{bpy})_2(\text{pbn}^{\bullet-})]^+$, the protonated one-electron-reduced species $[\text{Ru}(\text{bpy})_2(\text{pbnH}^*)]^{2+}$, the product $[\text{Ru}(\text{bpy})_2(\text{pbnHH})]^{2+}$, and the intermediate dimer species are found in Figure 8 (blue and black), Figure 5 (blue), and Figure 11 (red), respectively.

(45) Mayer, J. M. *Annu. Rev. Phys. Chem.* **2004**, *55*, 363–390.

(46) Yuasa, J.; Fukuzumi, S. *J. Am. Chem. Soc.* **2006**, *128*, 14281–14292.

It was found that formation of the one-electron-reduced species as a result of reduction by a solvated electron ($k = 3.0 \times 10^{10} \text{ M}^{-1} \text{ s}^{-1}$) or $\text{CO}_2^{\bullet-}$ ($k = 4.6 \times 10^9 \text{ M}^{-1} \text{ s}^{-1}$), or reductive quenching of an MLCT excited state, is followed by protonation of the reduced species. A $\text{p}K_a$ value of 11 was found for the resulting product from the pH dependence of the absorption spectrum as well as from electrochemical studies. Dimerization of $[\text{Ru}(\text{bpy})_2(\text{pbnH}^*)]^+$ ($k_{7a} = 2.2 \times 10^8 \text{ M}^{-1} \text{ s}^{-1}$) followed by decomposition of the dimer as well as cross reaction between singly reduced protonated and nonprotonated species ($k_8 = 1.2 \times 10^8 \text{ M}^{-1} \text{ s}^{-1}$) results in the formation of final product $[\text{Ru}(\text{bpy})_2(\text{pbnHH})]^{2+}$. In the case of the dimerization reaction, an intermediate was observed that decomposes thermally or upon additional reduction to form the final product. Formation of a π -stacking dimeric intermediate is proposed based on the electron density of the SOMO in the naphthyridine ligand, as evidenced by the analysis of spin densities obtained from DFT studies. The absence of a significant kinetic isotope effect (KIE) is also consistent with dimer formation ($\text{pH} < 9$). The lack of a KIE indicates that the disproportionation reaction ($\text{pH} > 9$) involves a stepwise pathway of electron transfer, followed by proton transfer. Finally, the pH-dependent decay of the excited state was found to be similar to the pH titration curve of the ground-state complex, consistent with the significantly shorter lifetime of the protonated excited-state species. We believe the equilibrium between the nonprotonated and protonated excited-state species is not established within the lifetime of the excited state.

Acknowledgment. We thank Take-aki Koizumi for his preliminary results. Work performed at Brookhaven National Laboratory was funded under contract DE-AC02-98CH10886 with the U.S. Department of Energy and supported by its Division of Chemical Sciences, Geosciences, & Biosciences, Office of Basic Energy Sciences.

Supporting Information Available: B3LYP-optimized Cartesian coordinates for three Ru species, TD-B3LYP calculated spectra of $[\text{Ru}(\text{bpy})_2(\text{pbn})]^{2+}$ and $[\text{Ru}(\text{bpy})_2(\text{pbn}^{\bullet-})]^+$, linear plots of observed rate constants of $[\text{Ru}(\text{bpy})_2(\text{pbn}^{\bullet-})]^+$ with e_{aq}^- and $\text{CO}_2^{\bullet-}$, plot of pH-dependent reaction rate constants between $\text{CO}_2^{\bullet-}$ and $[\text{Ru}(\text{bpy})_2(\text{pbn})]^{2+}$, UV-vis difference spectra of one-electron-reduced species $[\text{Ru}(\text{bpy})_2(\text{pbn})]^+$, plot of a second-order decay of $[\text{Ru}(\text{bpy})_2(\text{pbn}^{\bullet-})]^+$, UV-vis spectra of transient species, UV-vis spectra of the final product obtained after continuous exposure of $[\text{Ru}(\text{pbn})(\text{bpy})_2]^{2+}$ to $\text{CO}_2^{\bullet-}$ at 0.2 and 25 °C, and B3LYP-calculated interaction of the benzo[*b*]-1,5-naphthyridine anion radical ($\text{bn}^{\bullet-}$) and its conjugate acid radical (bnH^{\bullet}), and that of two bnH^{\bullet} radicals. This material is available free of charge via the Internet at <http://pubs.acs.org>.

IC702139N